6th European Conference on Computational Mechanics (ECCM 6)
7th European Conference on Computational Fluid Dynamics (ECFD 7)
11âĂŞ15 June 2018, Glasgow, UK

UNDERSTANDING TRANSONIC WEAPON BAY FLOWS

GAETAN J.M. LOUPY[1] and GEORGE N. BARAKOS[1]

[1] CFD Laboratory
University of Glasgow, G12 8QQ, UK
George.Barakos@glasgow.ac.uk

Key words: transonic cavity, CFD, weapon bay flow

Abstract. This paper presents some of the challenges in measuring and simulating cavity flows. The main characteristics of cavity flows are first described using experimental data, and beamforming is then used to provide good estimates of acoustics away from the cavity walls. Then, a simple model based on standing waves is introduced and it appears that the results capture some of the flow physics. Simulations of cavity flows and of store releases, and the importance of statistics in understanding the physics involved are shown.

1 INTRODUCTION

The growing demand for stealth operation of unmanned and manned combat aircraft, pushed engineers to move externally carried stores to weapon bays like the ones found on the F-35 and the B-52. Cavity flows generate strong acoustic fields, comprising broadband and tonal noise, called Rossiter modes[1]. Once the bay doors are open, the resonant cavity flow may be an obstacle to the safe store separation. The store is subject to unsteady loads, driving its trajectory, and the flow environment leads to store trajectory variability that is difficult to predict [2, 3]. In addition, cavity tones may excite the store and aircraft structures [4, 5], and may induce structural fatigue and failure.

This paper presents computational fluid dynamic (CFD), and theoretical results for transonic cavity flows. First, the main characteristics of cavity flows are presented using experiments available in the literature. Then, the difficulty to model this type of flows, and the implications for store release are shown. Afterwards, the ability of CFD to model cavity flow is shown and results are compared to experiments. Finally, results from coupled CFD/6DoF simulations of store release are presented, and the importance of statistical analysis of cavity flows is highlighted. In addition, recommendations for future studies are given.

2 UNCERTAINTY AND VARIABILITY IN CAVITY FLOWS

Experiments performed for the M219 cavity [6] provide a first insight into cavity flow uncertainty and variability. M219 has a length to depth ratio of 5, a width to depth ratio of 1, and a length of 0.51m. Experiments were carried out by Nightingale *et al.* [6] at Mach 0.85, and a Reynolds Re_L, based on the cavity length, of 6.5 million. Two cavities were tested, one has

two doors attached at its sides at an angle of 90 degrees (Figure 1), and the other has no doors. Experimental data was obtained using Kulite^{TM} pressure transducers at the cavity ceiling.

For the clean cavity configuration, a signal of 1910 travel times is available. However, three tests at the same conditions, named S1, S2 and S3 were performed for the M219 cavity with doors. They were sampled at different frequencies and have different durations. Table 1 presents a summary.

Figure 2 shows the SPL and OASPL at the ceiling mid-span for the different experimental data sets computed using the raw data. Vertical lines represent the Rossiter modes, that are empirical estimates of the cavity acoustic tones[7]. The SPL shows strong tones close to Rossiter modes 1, 2, 3 and 4 and a strong broadband noise. There is a finite number of tones of different amplitudes, and their distribution is not harmonic. S1 and S2 have similar SPL, and show less than 2dB differences in the OASPL. However, run S3 is different by 40dB in frequency, and 4dB in amplitude for the tones. In addition the OASPL is 3dB lower at the cavity front. In the following, run S2 is employed as it is the longest signal, and it agrees with the over-sampled signal S1 obtained two years earlier [6].

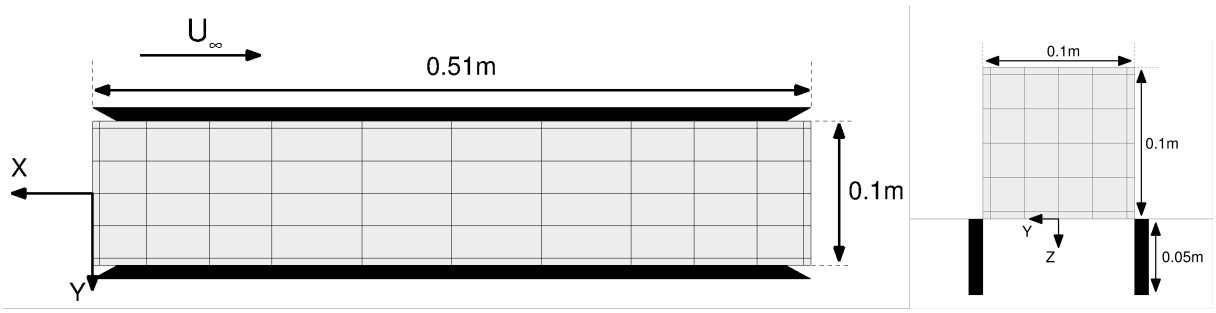

((a)) Bottom view ((b)) Downstream view

Figure 1: Schematic view of the M219 cavity with doors.

Name	Signal length (Travel Time)	Sampling (Hz)	Date
No Doors	1910	6.00	Oct 1991
Doors S1	1831	31.25	Sep 1999
Doors S2	16798	6.00	Mar 2001
Doors S3	1910	6.00	Sep 1999

Table 1: Available signals for CFD comparison.

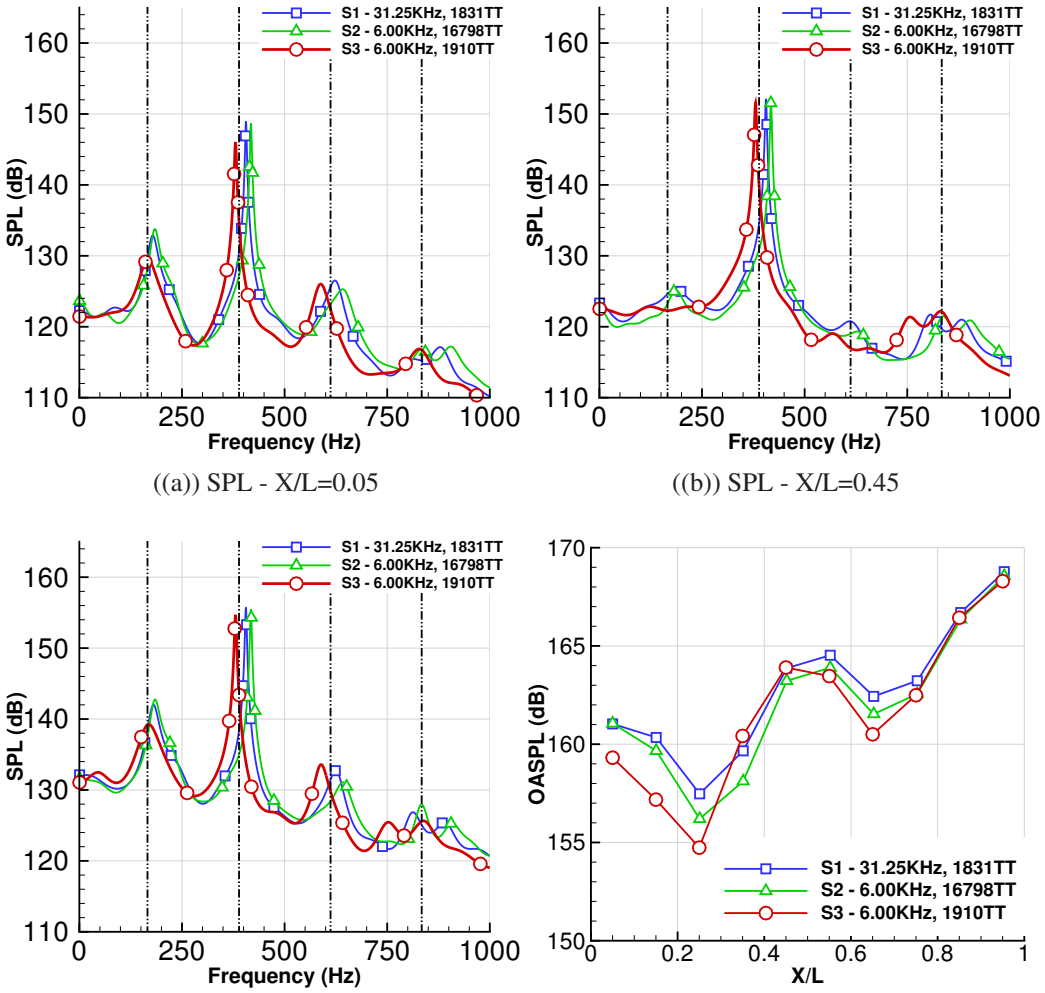

((a)) SPL - X/L=0.05

((b)) SPL - X/L=0.45

((c)) SPL - X/L=0.95

((d)) OASPL

Figure 2: M219 with door SPL and OASPL for three experimental signals.

The experiment is divided in windows of 25 travel times, and the maxima and minima over all windows are shown as envelope and vertical bars in figure 3. The envelope is wider than 20dB in SPL, and wider than 10dB in OASPL showing large fluctuations of the noise intensity over large time scales. Also, SPL, and OASPL are computed for signal sections of 25 travel times are shown for three selected windows. The time t=25.2s shows a large decrease of modes 1 and 2, while mode 3 is amplified. This shows that energy can move between tones, and this is called mode switching [8]. Those changes are related to the shape of the shear layer in time, and show that the noise field fluctuates over large time scales.

To dissect the pressure fluctuations over small time scales, Kegerise [8] used the wavelet transform to decompose the pressure signal in frequency, and time space. The wavelet transform $W_{\Psi}^{y}(f,t)$ [9] is a convolution of the signal $s(t)' = s(t) - \overline{s}$ with a scaled mother wavelet $\Psi(t)$

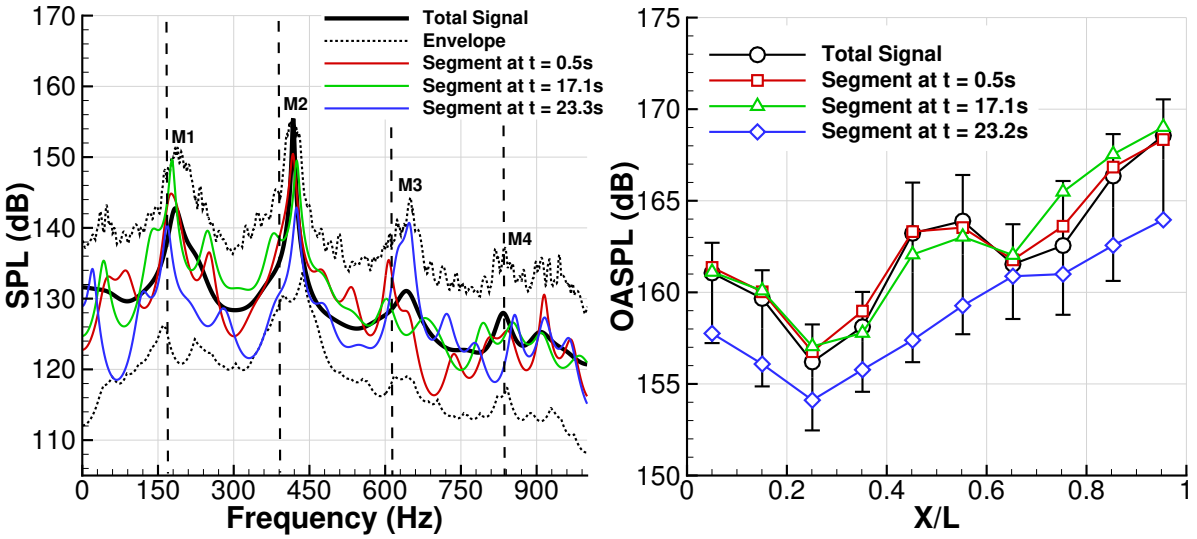

((a)) SPL at 95% of the cavity length

((b)) OASPL

Figure 3: Experimental SPL and OASPL at the ceiling mid-span and at different time with envelope.

conserving the sign of the signals in time and frequency:

$$W_{\Psi}^{y}(a,b) = \frac{1}{\sqrt{c_{\Psi}\,|a|}} \int_{-\infty}^{\infty} s'(t)\Psi\left(\frac{t-b}{a}\right) dt. \tag{1}$$

In the above equation, a is called the dilatation or the scale, b the translation parameter, $c_{\Psi} = \sqrt{\pi/\beta}$ and $\beta = \omega_0^2$. The dilatation a is related to the frequency f of the wavelet, the translation parameter b is related to the time shift t of the wavelet. The mother, or Gabor wavelet $\Psi(t)$ [9].

Band Integrated Wavelets (BIW) plots show the energy content within a particular frequency range and are calculated using the following equation:

$$BIW(t) = \int_{f_1}^{f_2} W_{\Psi}^{y}(f,t)^2 \tag{2}$$

where f_1 and f_2 are the lower and upper limits of the desired frequency range.

The wavelet envelope $|\overline{W_{\Psi}^{y}}|$ is the amplitude of the frequency in time, and is determined using the maximum of the absolute value of the wavelet transform $\overline{W_{\Psi}^{y}}$ over windows equal to half a period of the frequency. The wavelet amplitude in decibels W_{dB} is given by:

$$W_{dB}(f,t) = 20\ \mathrm{LOG}_{10}\left[\frac{|\overline{W_{\Psi}^{y}(f,t)}|^2}{p_{ref}}\right] \tag{3}$$

with p_{ref} the international standard for the minimum audible sound, which has the value of 2.10^{-5} Pa [10]. In the same way, Band Integrated Wavelets amplitude in decibel BIW_{dB} is given by:

$$BIW_{dB}(t) = 20\ \mathrm{LOG}_{10}\left[\int_{f_1}^{f_2} \frac{|\overline{W_{\Psi}^{y}(f,t)}|^2}{p_{ref}}\right] \tag{4}$$

Figure 4(a) shows an example for the experimental pressure of the M219 with doors at 95% of the ceiling mid-span. The pressure shows strong fluctuations at the tonal frequencies over small time scales. In addition, their amplitude appears to be modulated in time (Figure 4(b)). For example the first mode shows a maximum amplitude at travel time 580, while the second mode has a maximum at travel time 520. The pressure probes are analysed for several points along the cavity length, and the BIW is represented in figures 4(c) and 4(d) along the ceiling mid-span. The scalogram is integrated in windows of 20Hz centred on cavity modes 1 and 2. There are standing wave oscillations, characterised by nodes (minima of amplitude), and antinodes (maxima of amplitude). Furthermore, there is phase opposition between neighbouring antinodes. Figures 4(e) and 4(f) show that the mode amplitude modulation globally affects the entire cavity length.

Cavity flow fluctuations are the summation of small time scales (order of a travel time), and larger time scales (order of hundreds travel times) that create a non periodic flow as seen since the first experiments of Rossiter [1]. Other researchers suggest that these flows are pseudo-periodic [11]. Experimental measurements of cavity flows are difficult as multiple signals of the same cavity flow will not necessarily give exactly the same result. Numerical simulation and modelling are also difficult, as multiple time scales have to be correctly simulated to obtain an accurate cavity flow representation.

Experimental pressure data is limited to wall surfaces using kulite or pressure sensitive paint [12]. However, the main sources of noise are localised inside the shear layer are difficult to measure without intrusive techniques. Beamforming has been used in reference [13], and proved to be capable of capturing the noise field around the cavity using a limited number of probes, and the mean CFD flow-field to compute the noise propagation. Figure 5 shows a comparison between the BISPL computed over all grid points, and the beamforming computed using the acoustic array over the M219 cavity with doors. The beamforming reconstruction captured the strongest noise sources seen on the BISPL. This technique could be used in wind tunnels, coupling microphone array measurements, and PIV data. As a result, further cavity flows physics, and more data could be obtained for CFD validation.

3 MODELLING OF THE CAVITY FLOW PHYSICS

Cavity flow fluctuations are complex, and depend both on space and time, and so, modelling of such flows is challenging, and still remains an active research area. The fundamental goal is to identify the trigger of the tones, to help the design of flow control devices. Also, for routine engineering applications, estimates of the cavity flow noise field both in amplitude and frequency in a fast way, would be an advantage.

The first models appeared 70 years ago relying on experimental observations. Plumblee *et al.* [14] suggested that the turbulence growing in the shear layer provided a broadband noise source driving the cavity oscillations. The cavity response was to amplify small bands of frequencies, depending on the geometry and conditions. Rossiter [1] proposed a different model based on an acoustic feedback loop. Using shadowgraph images, he spotted vortices shed periodically from the front lip of the cavity. The vortices were travelling along the cavity length at the shear layer, generating acoustic waves when reaching the downstream wall. These acoustic waves travel upstream and interact with the shear layer, resulting in shedding of new vortices.

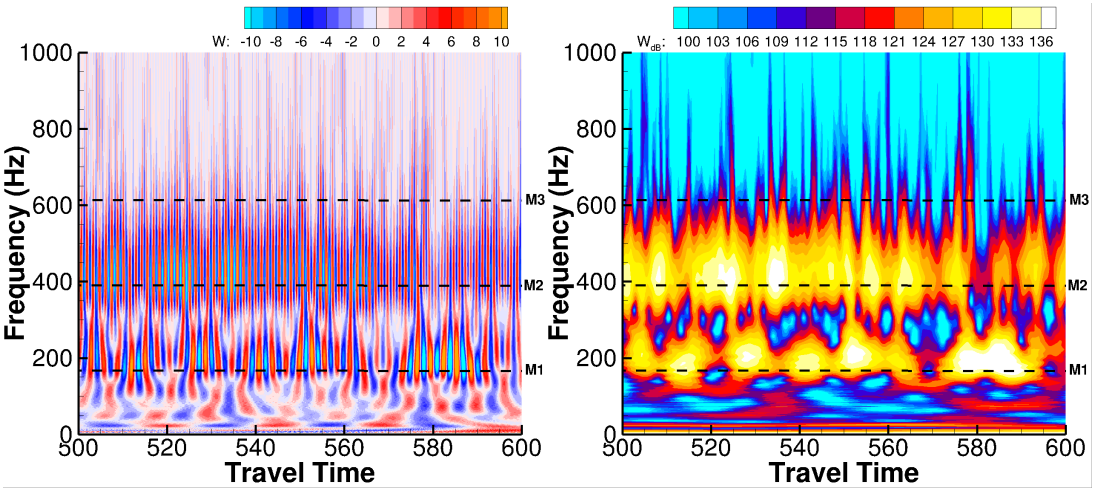

((a)) Scalogram at X/L=0.95 ((b)) Scalogram amplitude at X/L=0.95

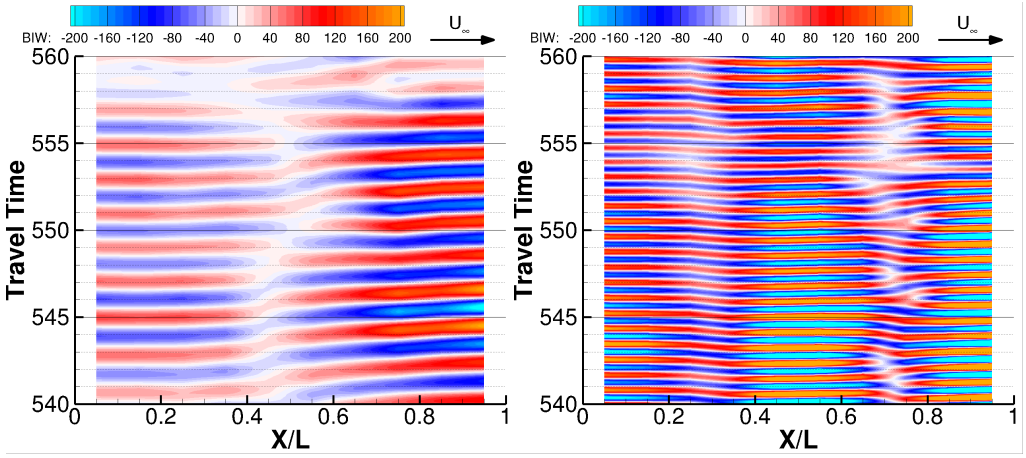

((c)) BIW of mode 1 ((d)) BIW of mode 2

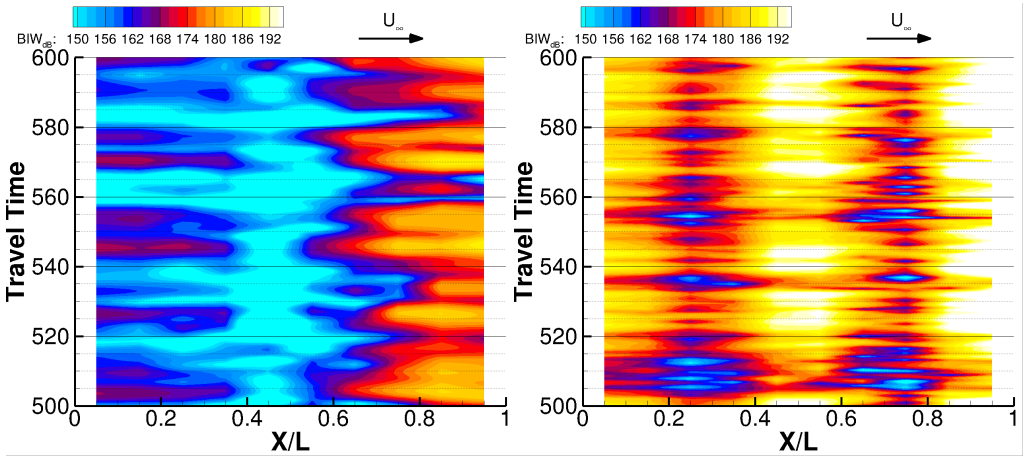

((e)) BIW amplitude of mode 1 ((f)) BIW amplitude of mode 2

Figure 4: Experimental scalogram at the ceiling mid-span.

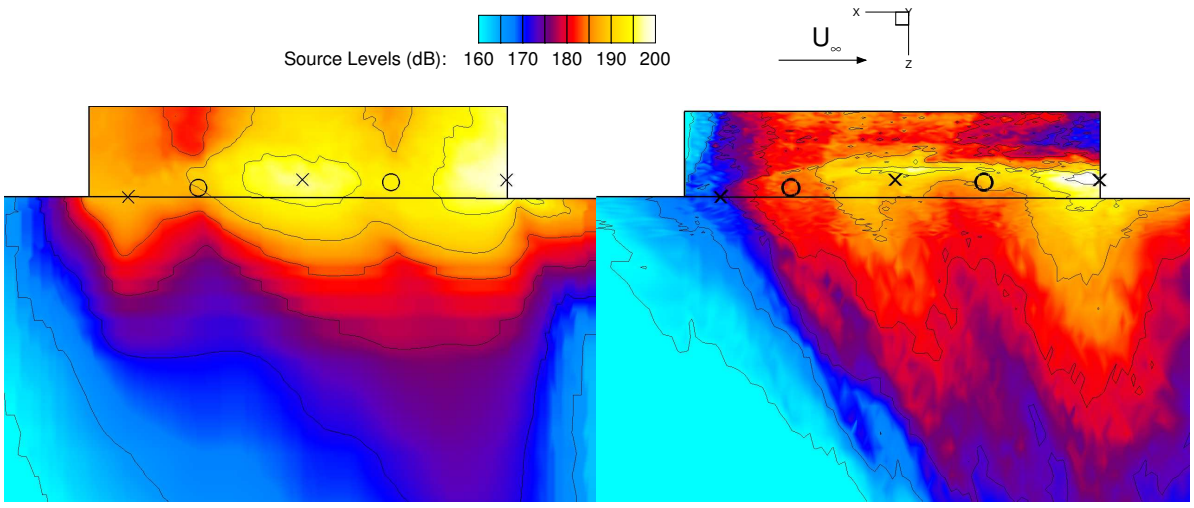

((a)) OASPL ((b)) Beamforming

Figure 5: Comparison between BISPL and beamforming reconstruction at cavity mid-span. Multi-spiral array with 31 microphones, placed at Z/L=1.5.

He proposed a formula based on those observations for estimating the tonal frequencies, that

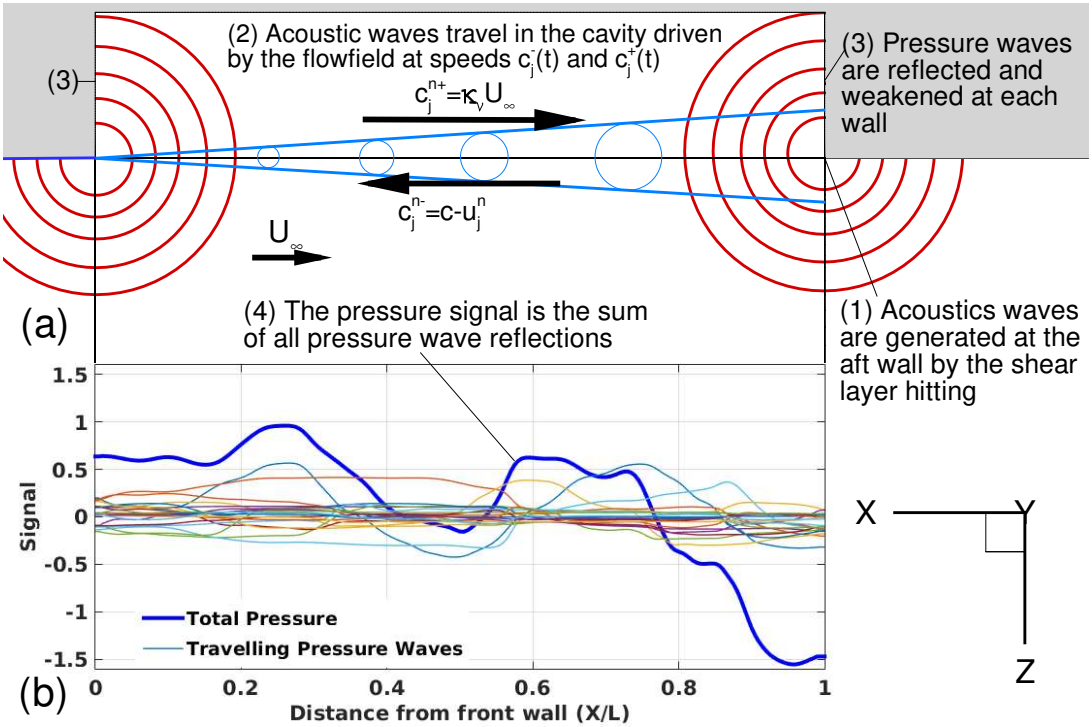

Figure 6: (a) Standing waves schematic, (b) Reflections and resulting pressures in cavity.

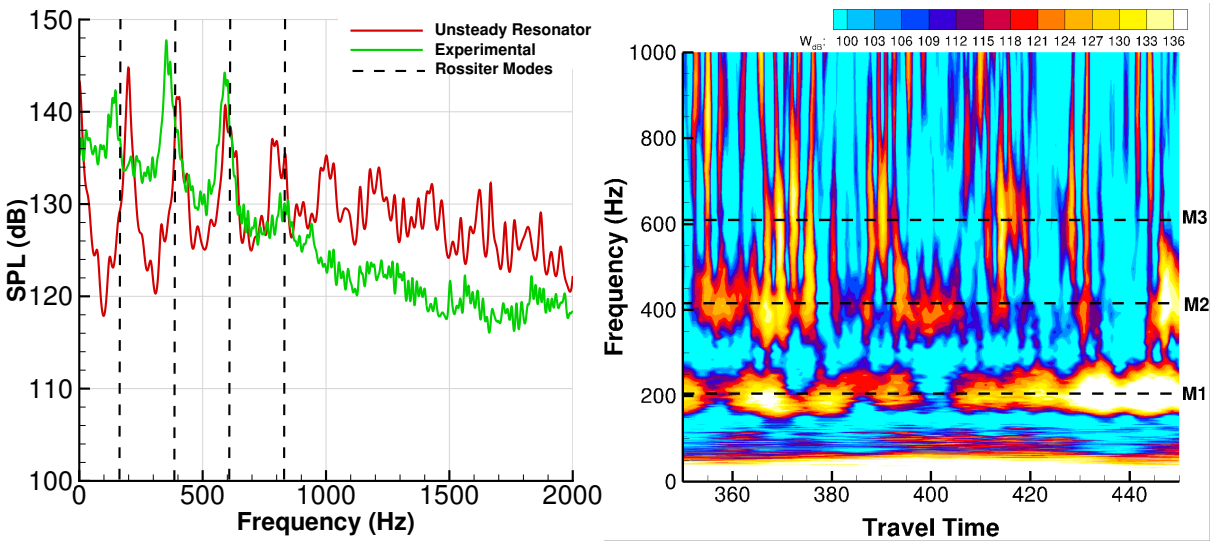

((a)) SPL ((b)) Wavelet Transform

Figure 7: Noise at 95%L of the M219 ceiling mid-span. L=0.51m.

was further modified by Heller [7] according to:

$$f_m = \frac{U_\infty}{L}\left[\frac{m-\alpha}{M_\infty\left(1+\left(\frac{\gamma-1}{2}\right)M_\infty^2\right)^{-1/2}+1/\kappa_\nu}\right] \tag{5}$$

where f_m is the frequency of mode m, U_∞ is the free-stream velocity, M_∞ is the free-stream Mach number, L is the cavity length, γ is the ratio of specific heats of the employed gas, α represents a phase shift, and κ_ν is the convection velocity coefficient of the vortices in the shear layer. These empirical constants have been tuned to fit experiments, and have the values 1.4, 0.25 and 0.57 respectively, for the case of the present study. Recent experimental data [11, 15] suggest that equation 5 can be valid even if κ_ν is different from the value found by Rossiter. As pointed out by Rossiter, this model is "merely an attempt to give a simple explanation of what is undoubtedly a highly complex motion" [1].

Other models rely on the excitation of the shear layer or on a small number of acoustic waves travelling inside the cavity [16, 17, 18]. They give a fair estimation of the tonal frequencies, but miss the tonal amplitude, the noise field shape, and all the unsteadiness described in section 2. The model from Alvarez [19] is better, providing the existence of the cavity modes.

Another model providing further insight is described in reference [13]. Based on the observation of standing waves in cavity flows, and the presence of numerous reflected waves in experiments [11, 20, 21, 22], it was assumed that the main mechanism driving the tone generation was similar to an one dimensional standing wave resonator, shown in figure 6. First, the pressure waves were generated as the shear layer impacted the downstream corner using a large range of frequencies (position (1) in figure 6). The pressure waves travelled towards the opposite wall (position (2) in figure 6), and were alternatively reflected (position (3) in figure 6) at the front, and at the aft walls, assuming an absorption by the reflection, and during the

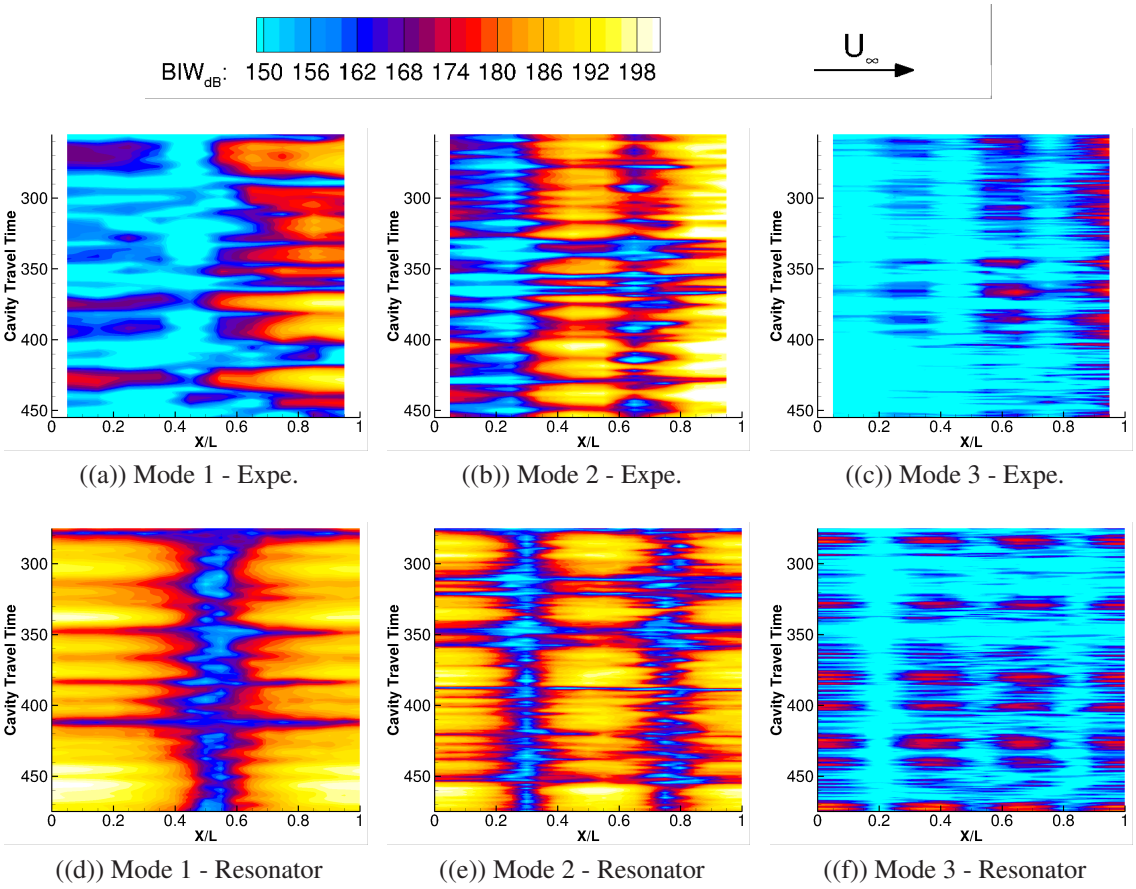

((a)) Mode 1 - Expe. ((b)) Mode 2 - Expe. ((c)) Mode 3 - Expe.

((d)) Mode 1 - Resonator ((e)) Mode 2 - Resonator ((f)) Mode 3 - Resonator

Figure 8: BIW envelope at ceiling mid-span for experimental and unsteady resonator.

wave travelling. The downstream waves travelled along with the shed vortices at about 69% of the free-stream velocity, while the upstream waves travelled at the sound speed reduced by the unsteady flow velocity computed with CFD. Finally, the resulting pressure signal was the sum of all reflections (curve (4) in figure 6).

In comparison with experiments, this model was capable to predict a finite number of tones, and the strong broadband noise (Figure 7(a)). In addition, the variation of the tone amplitude in time was captured (Figure 7(b)). More importantly, the spatial distribution of the modes along the cavity length was also predicted in agreement with experiments (Figure 8). Nevertheless, the relative modal amplitudes were not correct compared to the experiments, highlighting a missing part of the physics. This may be the shear layer motion that is driven by the strong pressure field in the cavity, and influences the generation of pressure waves at aft wall, creating a feedback loop. The model also needs detailed CFD data.

Overall, the available literature suggests that as the flow establishes, the shear layer hits the aft wall producing high frequency pressure waves reflecting inside the cavity. This wave superposition generates strong cavity modes at low frequencies due to the flowfield turbulence. Then, the cavity modes excite the shear layer motion, and this further amplifies the low frequencies in the pressure waves produced at aft wall. This feedback loop further amplifies the resonance,

and the cavity modes lock to their final frequencies.

Cavity flows involve very complex interactions between acoustics, turbulence, and shear layer motion that are difficult to model in a simple way. Engineering applications need accurate simulations, even with the presence of moving stores which can not be taken into account by the present models. Other researchers [23, 24, 25, 26] tried to simulate store releases with the $grid\ method$ measuring the time averaged loads on the store at different positions and attitudes by means of wind tunnel testing or CFD. Then the trajectory was computed feeding a 6DoF model with loads interpolated from the grid of aerodynamic influences. This method could be used as a rough estimate of the store trajectory, but is not accurate enough for store clearance certification that must account for cavity flow fluctuations evidenced in this section, and flow interactions with the store. Consequently, CFD appears to be a better candidate for engineering simulation of weapon bay flows.

4 CAVITY FLOW SIMULATION WITH CFD

The Helicopter Multi-Block (HMB3) [27, 28] code is used in the present work. The solver is described in references [29, 30, 31, 32] and has been extensively validated for cavity flows. DES is by far the most common way to account for the effect of turbulence in cavity flows. Nevertheless, DES is expensive, especially when several computations of store releases are required. Promising results with the SAS method [33] encouraged Babu *et al.* [29] to use this approach for weapon bay flows. Their results suggest that SAS captures the essential physics of the weapon bay, and at the same time, provides a significant reduction in CPU time by almost an order of magnitude. For this reason SAS is also used in the present work. In the following, the unsteady and averaged pressure field are compared for the M219 cavity with and without doors. CFD results for three grid densities of 13, 22 and 34 million points are compared to the experimental data for the cavity with doors. The computations used a dimensionless time-step of 0.01, and SAS are presented in table 2.

Name	Door Angle (deg)	Grid size (10^6 cells)	Cavity Travel Times
Coarse	90	13.2	25
Medium	90	22.3	25
Fine	90	33.9	30
No doors	-	23.0	30

Table 2: Details of the M219 computations.

Figure 9 shows the SPL comparison between CFD and experiments at three points at 5%L, 45%L, and 95%L on the cavity ceiling mid-span, for the M219 cavity with doors. Vertical black lines represent Rossiter's modes. The SPL results are in better agreement with the test data when the fine grid is used, capturing both tonal and broadband noise.

The time averaged C_p (Figure 10(a)) at the ceiling, and at the mid-span of the cavity, shows grid convergence, with negligible changes between the different grid densities. In the OASPL

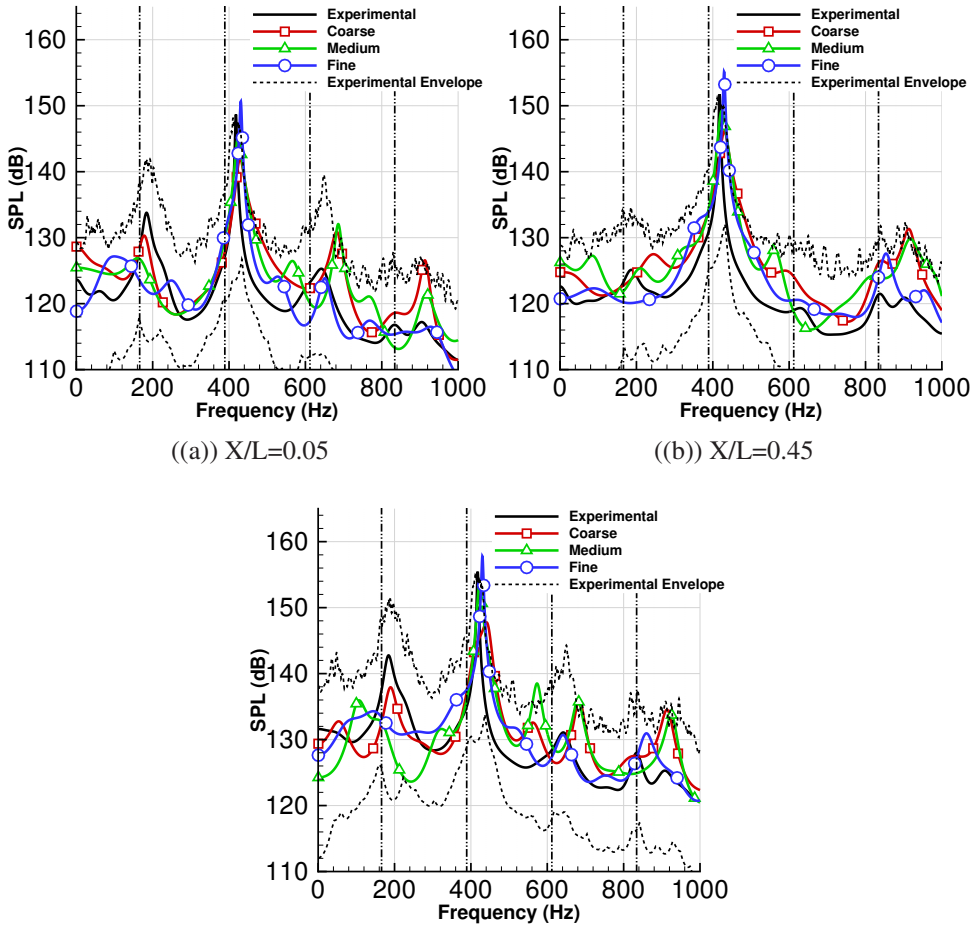

((a)) X/L=0.05

((b)) X/L=0.45

((c)) X/L=0.95

Figure 9: M219 with door SPL at ceiling mid-span for CFD and experiments.

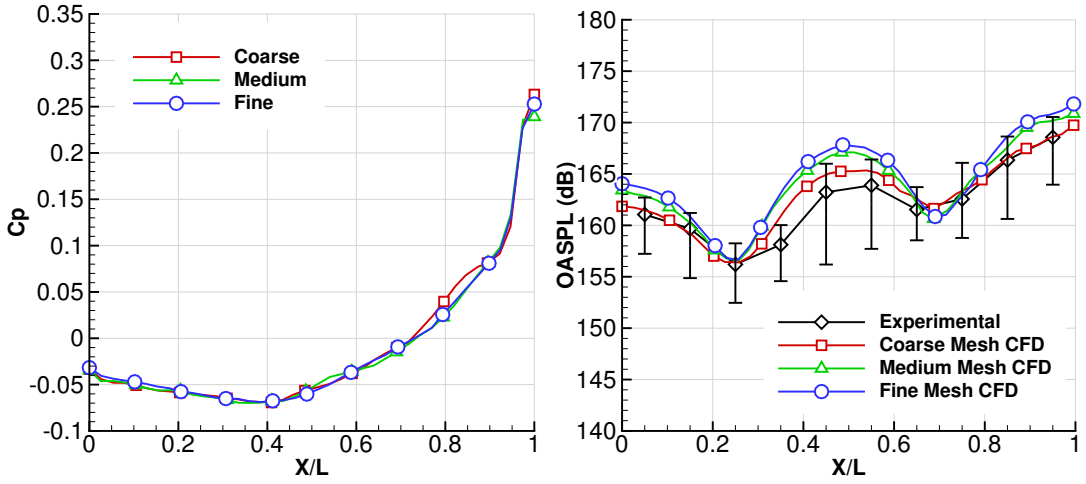

((a)) Mean Cp

((b)) OASPL

Figure 10: OASPL, and mean C_P along the M219 with doors ceiling mid-span.

(Figure 10(b)), the second Rossiter mode is dominant, with a W shape of the OASPL, as captured by the CFD and the experiments [34]. There is convergence towards the fine mesh solution, with a small relative difference of 1 dB between medium and fine grids.

The CFD results are compared with experiments for a cavity without doors in figure 11. Overall, the CFD captured well the differences between the door and no door configurations, including the strong increase of the second cavity mode with the doors, suggesting that SAS [35] is a suitable method for simulating this flow. Both cases with and without doors show a small overestimation of the OASPL, all along the cavity length. A large number of simulations performed with various models [36, 37, 38] had similar overestimation. This may be due to experimental errors, the signal length, as well as limitations of the SAS [35] and DES [39] approaches.

The time averaged stream-wise velocity is compared in figure 12 between CFD and PIV experiments [40] for the M219 cavity without doors. The CFD results agree well with the experiments for the stream-wise velocity component, showing the development of the shear layer along the cavity length.

The wavelet transform is used to perform spatio-temporal validation of the CFD signals. The pressure probes are analysed, and the Banded Integral Wavelet (BIW) is given in figure 13 for 25 travel times, along the ceiling centre line. The BIW is integrated in windows of 20Hz centred on the first, and second cavity modes. There is a fair agreement of the CFD with the experiments, showing standing wave oscillations with respectively a tick, and a W shape for modes 1 and 2.

The BIW envelope is shown figure 14. The CFD signal agrees with the experiments showing the characteristic shape of the first mode, with two antinodes at the front, and the aft wall. The second mode shows the W shape seen on the OASPL. Also, both experiments and CFD show global fluctuations of the amplitude along the cavity length.

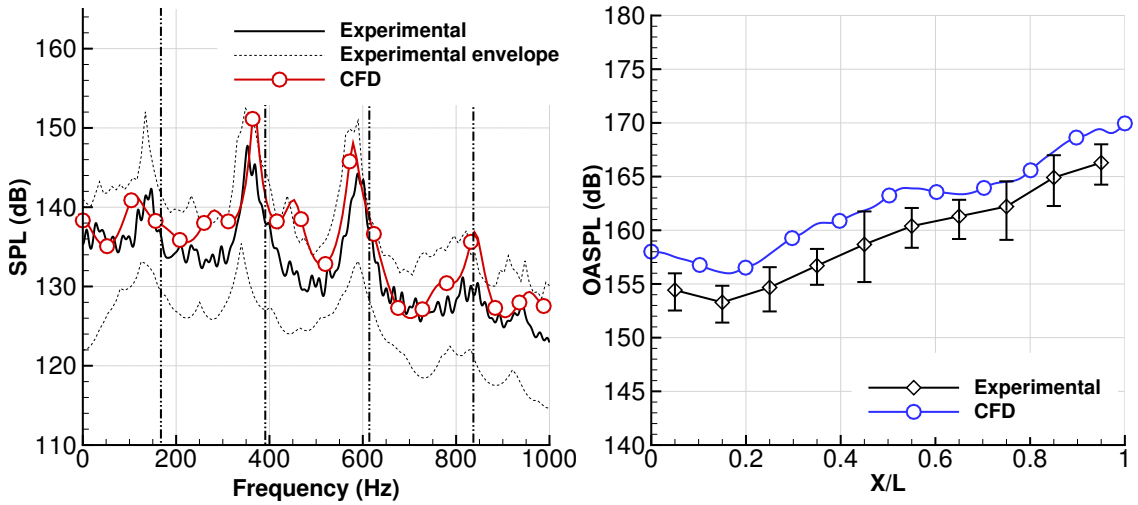

((a)) SPL ((b)) OASPL

Figure 11: Noise along the no doors M219 cavity ceiling mid-span.

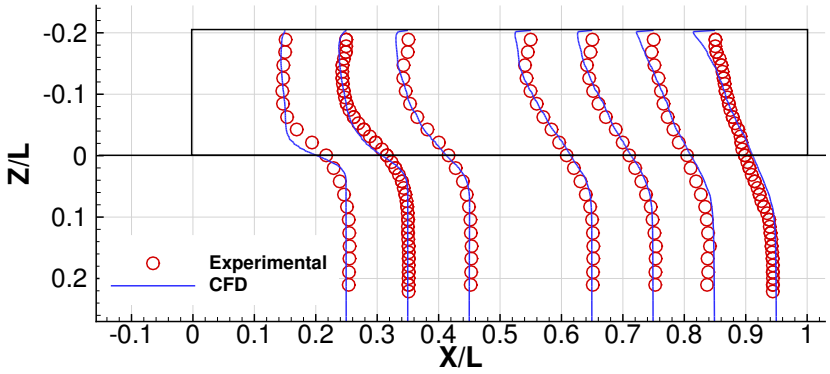

Figure 12: Time averaged stream-wise velocity at the mid-span of the cavity along vertical lines.

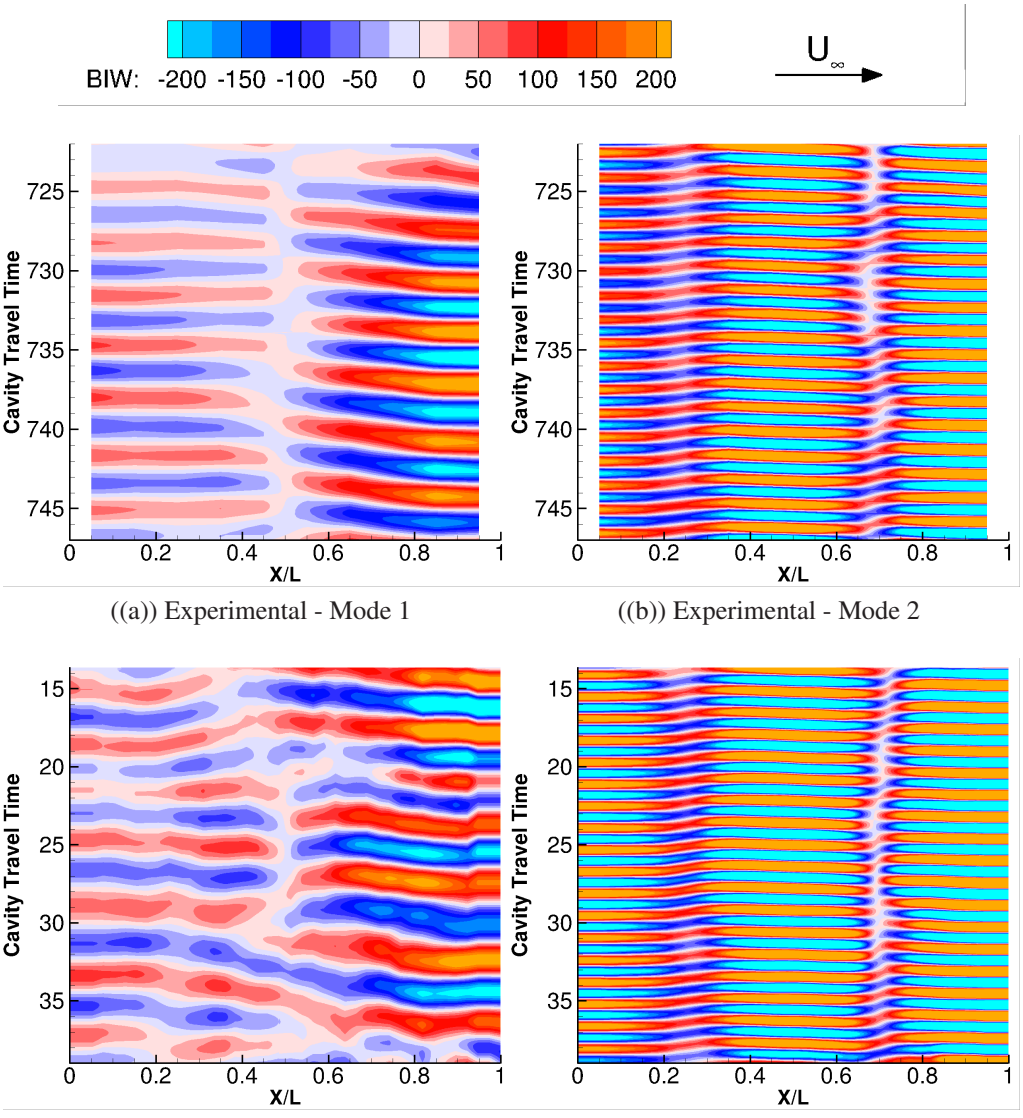

((a)) Experimental - Mode 1

((b)) Experimental - Mode 2

((c)) CFD - Mode 1

((d)) CFD - Mode 2

Figure 13: BIW at the cavity ceiling centre-line for modes 1 and 2.

Overall, the SAS turbulence model shows reasonable agreement with experiments for the transonic cavity pressure field on average and in terms of spatio-temporal components.

5 STATISTICAL ANALYSIS OF STORE RELEASES

Store release simulations are performed here and include CFD and Six Degree of Freedom (6DoF) flight mechanics. A small number of CFD tools are able to perform this type of simulation and were used for realistic [41, 42, 43], and prismatic [26, 44, 45] weapon bays. Results show variability for most of the cases as LES, DES, and SAS are able to resolve the turbulence within the cavity [37]. Nevertheless, a small number of numerical releases were performed for each case, and none of the published works provided any further insight on the mechanism that

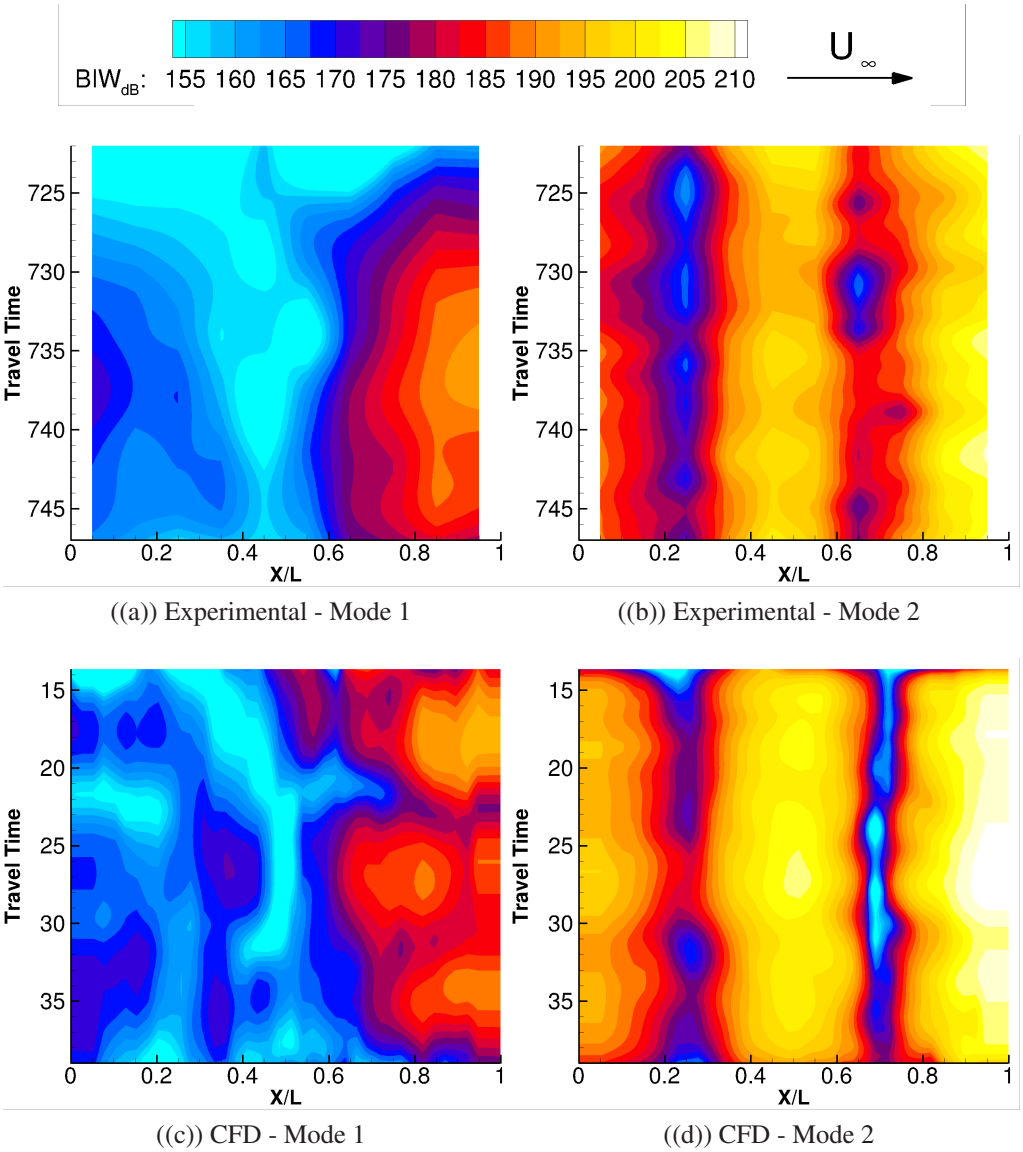

((a)) Experimental - Mode 1

((b)) Experimental - Mode 2

((c)) CFD - Mode 1

((d)) CFD - Mode 2

Figure 14: BIW amplitude at the cavity ceiling centre-line for modes 1 and 2.

drives the store trajectory in terms of average and variability. This is because the non periodicity of this flow makes every release different.

Reference [3] tackles this difficulty in performing twenty numerical releases and considering the statistics of the ensemble. The computations were carried using HMB3 and the Scale-Adaptive Simulation. The free-stream Mach number was 0.85 and the Reynolds number based on the cavity length (Re_L) was 6.5 million. The cavity had a length to depth ratio of 7, and was 3.59m long, and 1.03m wide. The store was 90% of the cavity length with four fins in a cross configuration (Figure 15). The store release includes three phases. At $carriage$ (Z/D=-0.5), the store is fixed while the flow is allowed to develop. Then, during the $stroke\ phase$, the store is pushed towards the cavity opening. During this phase, a vertical velocity of 5m/s is imposed on the store, with other degrees of freedom set to zero. This phase ends when the stroke length is reached. Finally the store is free to move under the aerodynamic forces.

The trajectory variability (Figure 16) was negligible for the translations, while the rotations, mainly in roll, varied widely. Filtering the simulation results, revealed that the vertical displacement of the store was driven by the lower frequencies related to the ejection velocity and gravity. On the other hand, the rotation variability came from the tonal fluctuations, and only the roll angle was driven by the finest fluctuations in the flowfield related to turbulence. The receptivity of the store to all the time scales of the cavity flow explained that each trajectory was unique.

A statistical metric was proposed to identify the minimum number of simulations necessary for capturing the mean of the trajectories as the maximum of the normalised difference between the average of n+1, and n trajectories:

$$\Delta_\mu = \frac{max|\mu(t, n+1) - \mu(t, n)|}{W_e} \tag{6}$$

with $\mu(t, n)$ the average of n trajectories, where t covers the complete time of simulation. The envelope of the trajectory was defined as the maximum difference between minimum, and maximum over all releases and all store vertical positions. W_e was the largest envelope width over all positions, and indicated by dashed lines in figure 16. A trajectory component was considered as converged if the difference (Δ_μ) between two consecutive averages was less than 5%. The number of releases to converge the statistics depends on the order of the trajectories. To minimise this effect, Δ_μ was computed for 100.000 random trajectory permutations. For each permutation, the number of releases required to converge the statistics was computed, and the

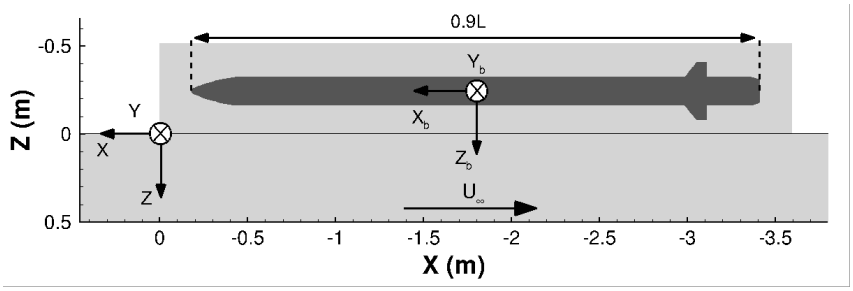

Figure 15: Geometry, cavity axes, and the store at carriage position.

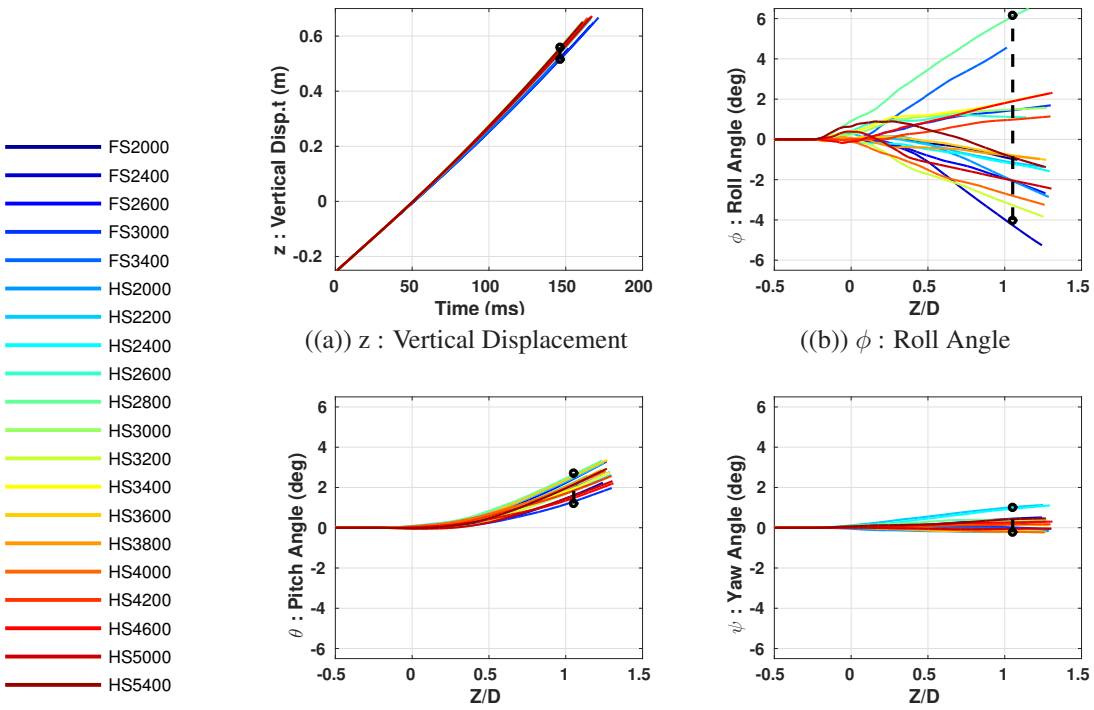

((a)) z : Vertical Displacement

((b)) ϕ : Roll Angle

((c)) θ : Pitch Angle

((d)) ψ : Yaw Angle

Figure 16: Trajectory of full and half stroke cases.

cumulative plot in figure 17 indicates the number of converged permutations in respect to the number of releases included in the mean. For the store at hand, 17 trajectories were necessary, mainly due to variability in roll associated with its low roll inertia.

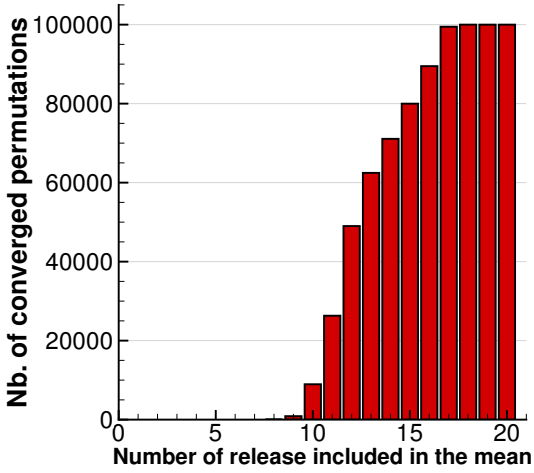

Figure 17: Number of converged permutation as function of the number of releases included in the mean.

Using the averaged flow data, the trajectory phases were identified and the role of the pressure field inside the cavity was clarified. For example, figure 18 shows the vertical force, and pitching moment averages considering all times of the simulations from stroke initiation until a common point in time corresponding to the shortest of the simulated trajectories. The load peaks were identified and are the result of the interaction between the store and the shear layer.

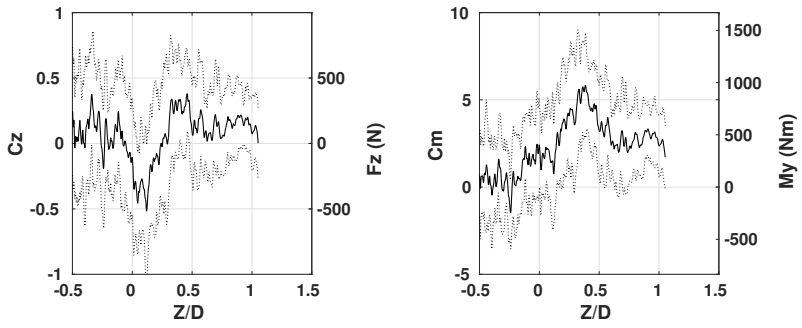

((a)) C_z : Vertical Force ((b)) C_m : Pitching Moment

Figure 18: Averaged translations and rotations with half and full stoke releases.

HMB3 proved to be efficient for engineering computations of store release, using a reasonable amount of CPU. In addition, the obtained large CFD data sets gave more insight in the physics involved.

The next step in this effort should be to produce more experimental data for CFD validation. HMB3 results agreed with captive trajectory system (CTS) experiments of a store released from a wing [46], and from a cavity flow [47]. However, CTS experiments [47] have the drawback to work by integrating the loads on the store, before moving it, neglecting the effect of the smaller scales of the cavity flow. The only way to validate a CFD code for the trajectory variability from a weapon bay, is to perform free releases in wind tunnels, or during flight test to take all flow scales into account. Flight tests have been performed by the Institute of High Performance Computing Application to Air Armament (IHAAA) [48], and wind tunnel tests by Boeing [49] and by the US Air Force [2]. Nevertheless, this data involved a small number of releases, was not disclosed to public[48], was affected by scaling effects[2], and the test conditions were not properly reported[49].

Future store release experiments must consider a large cavity of at least a meter long to minimise scaling effects. Additionally, the number of releases to perform should be determined using the criteria of equation 6, to ensure that statistics are converged. Then, it will be possible to compare standard deviation, and the average trajectory between CFD and experiments.

6 CONCLUSIONS

This paper gave a detailed view of the difficulties in measuring and simulating weapon bays flows. Cavity flow fluctuations include a large range of time scales. This creates a non-periodic flow that is unique for each weapon bay door opening. Cavity flows are difficult to model, as they are the result of the interaction between acoustics, turbulence and shear layer motion.

Engineering applications need CFD to take into account complex geometries, and store interactions with the cavity flow. Strong coupling between CFD and 6DoF methods can be used to simulate store trajectory variability, and to build statistics within a reasonable time. This is the best way, at present, to make understanding from the trajectories that are driven by all cavity flow scales. Future work should focus on experimental tests to better validate CFD codes for the store trajectory variability.

Acknowledgements

The financial support of MBDA UK Ltd. is gratefully acknowledged. The use of the EPSRC funded ARCHIE-WeSt High Performance Computer (EPSRC grant no. EP/K000586/1) is also gratefully acknowledged.

NOMENCLATURE

Acronyms

BIW Banded Integrated Wavelet

CFD Computational Fluid Dynamics

DES Detached Eddy Simulation

HMB Helicopter Multi-Block

LES Large Eddy Simulation

OASPL Overall Sound Pressure Level

PIV Particle Image Velocimetry

SAS Scale Adaptive Simulation

SPL Sound Pressure Level

TT Travel Time

6DoF Six-Degree of Freedom

Greek Symbols

α Rossiter Phase shift (-)

Δ_μ Statistical convergence index (-)

κ_ν Rossiter convection velocity coefficient (-)

γ Ratio of specific heats (-)

$\mu(t,n)$ Average of n trajectories

ω_0 Pulsation ($2\pi f$) (1/s)

ϕ, θ, ψ Roll, pitch and yaw angles (deg)

$\Psi(t)$ Mother wavelet (-)

Latin Symbols

$p'(\mathbf{x},t)$ Unsteady pressure time signal [Pa]

R Propeller Radius [m]

X Fuselage longitudinal coordinate [m]

C_x, C_y, C_z Axial, side and normal force coefficients (-)

C_l, C_m, C_n Rolling, pitching and yawing moment coefficients (-)

c_j^{n-}, c_j^{n+} Upstream, and downstream wave speed at point j and time n (m/s)

C_p Pressure coefficient (-)

D Cavity depth (m)

f_m Rossiter mode frequency (Hz)

I_x**,** I_y**,** I_z Moment of inertia of the store ($kg.m^2$)

L Cavity length (m)

m Rossiter mode number (-)

M_∞ Free-stream Mach number (-)

p, q, r Roll, pitch and yaw rates (deg/s)

p Pressure (Pa)

p_{ref} International standard minimum audible sound ($2.10^{-5}Pa$)

Re_L Reynolds number based on cavity length (-)

u, v, w Velocity components (m/s)

t Time (s)

U_∞ Free-stream Velocity (m/s)

u_j^n Axial flow-field velocity at point j and time n (m/s)

W Cavity width (m)

W_e Maximum envelope width

W_Ψ^y Wavelet transform

X, Y, Z Earth reference coordinates (m)

X_b, Y_b, Z_b Store reference coordinates (m)

References

[1] J. E. Rossiter. Wind Tunnel Experiments on the Flow Over Rectangular Cavities at Subsonic and Transonic Speeds. Technical Report 64037, Royal Aircraft Establishment, Bedford, UK, October 1964.

[2] J.D. Merrick and M.F. Reeder. Sphere release from a rectangular cavity at mach 2.22 freestream conditions. *Journal of Aircraft*, 53(3):822–829, 2016. doi:10.2514/1.C033636.

[3] G.J.M. Loupy, G.N. Barakos, and N.J. Taylor. Assessment of store release variability from weapon bay using scale adaptive simulation. *AIAA Journal*, 2017. Accepted for Pubication.

[4] J.L. Wagner, K.M. Casper, S.J. Beresh, P.S. Hunter, R.W. Spillers, and J.F. Henfling. Response of a store with tunable natural frequencies in compressible cavity flow. *Journal of Aircraft*, 53(4): 2351–2360, 2016. doi:10.2514/1.J054688.

[5] S.V. Babu, G.J.M. Loupy, F. Dehaeze, G.N. Barakos, and N.J. Taylor. Aeroelastic simulations of stores in weapon bays using detached-eddy simulation. *Journal of Fluids and Structures*, 66: 207–228, October 2016. doi:10.2514/6.2017-3252.

[6] D.A. Nightingale, J.A. Ross, and G.W. Foster. Cavity Unsteady pressure measurements - Examples from Wind-Tunnel Tests. Technical Report Version 3, Aerodynamics & Aeromechanics Systems Group, QinetiQ, Bedford, UK, November 2005.

[7] H.H. Heller, D.G. Holmes, and E.E. Covert. Flow-Induced Pressure Oscillations In Shallow Cavities. *Journal of Sound and Vibration*, 18(4):545 – 553, 1971. ISSN 0022-460X. doi:10.1016/0022-460X(71)90105-2.

[8] M.A. Kegerise, E.F. Spina, S. Garg, and L.N. Cattafesta. Mode-switching and nonlinear effects in compressible flow over a cavity. *Physics of Fluids*, 16(3):678–687, 2004. doi:10.1063/1.1643736.

[9] R. Bussow. An algorithm for the continuous morlet wavelet transform. *Mechanical Systems and Signal Processing*, 21(8):2970–2979, 2007. doi:10.1016/j.ymssp.2007.06.001.

[10] A.D. Pierce. *Acoustics: An Introduction to its Physical Principles and Applications*. Woodbury, New York: Acoustical Society of America, 1989. ISBN 0883186128.

[11] R.F. Schmit, J.E. Grove, F. Semmelmayer, and M. Haverkamp. Nonlinear feedback mechanisms inside a rectangular cavity. *AIAA Journal*, 52(10):2127 – 2142, 2014. doi:10.2514/1.J052804.

[12] W. Flaherty, T.M. Reedy, G.S. Elliott, J.M. Austin, R.F. Schmit, and J. Crafton. Investigation of cavity flow using fast-response pressure-sensitive paint. *AIAA Journal*, 52(11):2462–2470, 2014. doi:10.2514/1.J052864.

[13] G.J.M. Loupy and G.N. Barakos. Acoustic field around a transonic cavity flow. *International Journal of AeroAcoustics*, 16(6), 2017. doi:10.1177/1475472X17730459.

[14] Plumblee H.E., Gibson J.S., and L.W. Lasstier. A theoretical and experimental investigation of the acoustic response of cavities in an aerodynamic flow. Technical Report WADD-TR-61-75, US Air Force, 1962.

[15] J.L. Wagner, K.M. Casper, S.J. Beresh, S. Arunajatesan, J.F. Henfling, R.W. Spillers, and B.O. Pruett. Relationship between acoustic tones and flow structure in transonic cavity flow. In *Proceedings of the 45th AIAA Fluid Dynamics Conference, AIAA AVIATION Forum*, number AIAA 2015-2937, Dallas, TX, United States, 2015. American Institute of Aeronautics and Astronautics Inc. doi:10.2514/6.2015-2937.

[16] A.J. Bilanin and E.E. Covert. Estimation of Possible Excitation Frequencies for Shallow Rectangular Cavities. *AIAA Journal*, 11(3):347–351, March 1973. doi:10.2514/3.6747.

[17] C.K.W. Tam and P.J.W. Block. On the tones and pressure oscillations induced by flow over rectangular cavities. *Journal of Fluid Mechanics*, 89(2):373–399, 1978. doi:10.1017/S0022112078002657.

[18] T. Handa, H. Miyachi, H. Kakuno, T. Ozaki, and S. Maruyama. Modeling of a feedback mechanism in supersonic deep-cavity flows. *AIAA Journal*, 53(2):420–425, 2015. doi:10.2514/1.J053184.

[19] J.O. Alvarez, E.J. Kerschen, and A. Tumin. A theoretical model for cavity acoustic resonances in subsonic flow. In *Proceedings of the 10th AIAACEAS Aeroacoustics Conference*, number AIAA 2004-2845, Manchester, UK, 2004. American Institute of Aeronautics and Astronautics Inc. doi:10.2514/6.2004-2845.

[20] H.H. Heller and D.B. Bliss. Aerodynamically Induced Pressure Oscillations in Cavities – Physical Mechanisms and Suppression Concepts. Technical Report AFFDL-TR-74-133, Air Force Flight Dynamics Laboratory, 1975.

[21] M.A. Kegerise, E.F. Spina, and L.N. Cattafesta. An experimental investigation of flow-induced cavity oscillations. In *Proceedings of the 30th Fluid Dynamics Conference*, number AlAA 99-3705, Norfolk,VA, United States, 1999. doi:10.2514/6.1999-3705.

[22] S. Garg and L.N. Cattafesta III. Quantitative schlieren measurements of coherent structures in a cavity shear layer. *Experiments in Fluids*, 30(2):123–134, 2001. doi:10.1007/s003480000147.

[23] R. Johnson, M.B. Davis, and D. Finley. Relaxed Fidelity CFD Methods Applied to Store Separation Problems. Williamsburg, VA, USA, 7–9 June 2004. RTO AVT Symposium on "Functional and Mechanical Integration of Weapons and Land and Air Vehicles", Published in RTO-MP-AVT-108.

[24] M. Smith and S. Schwimley. X-45A/Small Smart Bomb Separation Analysis. In *Proceedings of the 44^{th} AIAA Aerospace Sciences Meeting and Exhibit*, number AIAA 2006-827, Reno, Nevada, USA, 9-12 January 2006. doi:10.2514/6.2006-827.

[25] L.P. Finney. *Investigation of Cavity Flow Effects on Store Separation Trajectories. Trident Scholar Project Report No. 388*. PhD thesis, U.S. Naval Academy, May 2010.

[26] M.B. Davis, P. Yagle, B.R. Smith, K.N. Chankaya, and R.A. Johnson. Store Trajectory Response to Unsteady Weapons Bay Flowfields. In *Proceedings of the 47th AIAA Aerospace Sciences Meeting*, number AIAA 2009-547, Orlando, FL, United States, 2009. doi:10.2514/6.2009-547.

[27] R. Steijl, G. N. Barakos, and K. Badcock. A framework for cfd analysis of helicopter rotors in hover and forward flight. *International Journal for Numerical Methods in Fluids*, 51(8):819–847, 2006. doi: 10.1002/d.1086.

[28] S. J. Lawson, R. Steijl, M. Woodgate, and G. N. Barakos. High performance computing for challenging problems in computational fluid dynamics. *Progress in Aerospace Sciences*, 52(1):19–29, 2012. doi: 10.1016/j.paerosci.2012.03.004.

[29] S.V. Babu, G. Zografakis, G. N. Barakos, and A. Kusyumov. Evaluation of scale-adaptive simulation for transonic cavity flows. *International Journal of Engineering Systems Modelling and Simulation*, 8(2):106–124, 2016. doi:10.1504/IJESMS.2016.075510.

[30] M. Jarkowski, M.A. Woodgate, G.N. Barakos, and J. Rokicki. Towards Consistent Hybrid Overset Mesh Methods for Rotorcraft CFD. *International Journal for Numerical Methods in Fluids*, 74(8): 543–576, 2014. ISSN 1097-0363. doi:10.1002/fld.3861.

[31] G.J.M. Loupy and G.N. Barakos. Processing and analysis methods for transonic cavity flow. *Physics of Fluids*, 29(16), 2017. doi:10.1063/1.4995461.

[32] G.N. Barakos, S.J. Lawson, R. Steijl, and P. Nayyar. Numerical Simulations of High–Speed Turbulent Cavity Flows. *Flow, Turbulence and Combustion*, 83(4):569–585, December 2009. doi:10.1007/s10494-009-9207-1.

[33] F.R. Menter and Y. Egorov. The Scale-Adaptive Simulation Method for Unsteady Turbulent Flow Predictions. Part 1: Theory and Model Description. *Flow, Turbulence and Combustion*, 85(1): 113–138, 2010. ISSN 1386-6184. doi:10.1007/s10494-010-9264-5.

[34] B.H.K. Lee. Effect of Captive Stores on Internal Weapons Bay Floor Pressure Distributions. *Journal of Aircraft*, 47(2):732–735, March-April 2010. doi:10.2514/1.46684.

[35] F.R. Menter, M. Kuntz, and R. Bender. A Scale-Adaptive Simulation Model for Turbulent Flow Predictions. In *Proceedings of the 41st Aerospace Sciences Meeting and Exhibit*, Reno, Nevada, USA, 6-9 January 2003. doi:10.2514/6.2003-767.

[36] Richard Allen, Fred Mendonça, and David Kirkham. Rans and des turbulence model predictions of noise on the m219 cavity at m=0.85. *International Journal of Aeroacoustics*, 4(1):135–151, 2015. doi:10.1260/1475472053730039.

[37] Shia-Hui Peng. *M219 Cavity Flow*, volume 103, pages 270–285. Springer International Publishing, Berlin, Heidelberg, 2009. doi:10.1007/978-3-540-92773-0.

[38] L. Temmerman, B. Tartinville, and Ch. Hirsch. *URANS Investigation of the Transonic M219 Cavity*, pages 471–481. Springer Berlin Heidelberg, Berlin, Heidelberg, 2012. doi:10.1007/978-3-642-31818-4_41.

[39] J. Smagorinsky. General Circulation Experiments with the Primitive Equations. *Monthly Weather Review*, 91(3):99–164, March 1963.

[40] J. A. Ross. Piv measurements of the flowfields in an aerodynamically deep cavity. Technical report, Aerodynamics & Aeromechanics Systems Group, QinetiQ, Bedford, UK, October 2002.

[41] R. Spinetti and B. Jolly. Time-Accurate Numerical Simulation of GBU-38s Separating from the B-1B Aircraft with Various Ejector Forces, Store Properties, and Load-Out Configurations - IHAAA Store Separation Cavity (SSC) Project. In *Proceedings of the 46th AIAA Aerospace Sciences Meeting and Exhibit*, number AIAA 2008-0187, Reno, NV, United States, 7–10 January 2008. doi:10.2514/6.2008-187.

[42] W.L. Sickles, T.L. Hand, C.H. Morgret, J.S. Masters, and A.G. Denny. High-fidelity, time-accurate cfd store separation simulations from a b-1b bay with comparisons to quasi-steady engineering methods. In *Proceedings of the 46th AIAA Aerospace Sciences Meeting and Exhibit*, number AIAA 2008-186, Reno, NV, United States, 7-10 January 2008. doi:10.2514/6.2008-186.

[43] J. Lee, A. Piranian, J. Martel, D. Crowe, and M. Rizk. Store Separations in Jet Flow Environments. In *Proceedings of the 48th AIAA Aerospace Sciences Meeting*, number AIAA 2010-510, Orlando, Florida, USA, 4-7 January 2010. doi:10.2514/6.2010-510.

[44] T.J. Flora, M.F. Reeder, A. Lofthouse, and N. Kraft. Dynamic store release of ice models from a cavity into mach 2.9 flow. *Journal of Aircraft*, 51(6):1927–1941, 2014. doi:10.2514/1.C032459.

[45] D. Kim, J. Choi, and O. Kwon. Detached eddy simulation of weapons bay flows and store separation. *Computers and Fluids*, 121:1–10, 2015. doi:10.1016/j.compfluid.2015.07.022.

[46] J.H. Fox. Generic Wing Pylon, and Moving Finned Store. TN. 37389-6001. Arnold Engineering Development Center (AEDC), Arnold AFB, USA, 2000.

[47] R.E. Dix and R.C. Bauer. Experimental and theorical study od cavity acoustics. Technical Report AEDC-TR-99-4, Tenessee, United States, April 2000.

[48] Donald Atkins. Flight test results of a gbu-38 separating from the b-1b aircraft. In *Proceedings of the 46th AIAA Aerospace Sciences Meeting and Exhibit*, number AIAA 2008-184, Reno, Nevada, United States, 7-10 January 2008. American Institute of Aeronautics and Astronautics Inc. doi:10.2514/6.2008-184.

[49] A.W. Cary and L.P. Wesley. Airframe integration of modern stores (aims) delivery order 0031: Phase ii and iii analytical predictions and validation testing. Technical Report AFRL-VA-WP-TR-2006-3079, Dayton, OH, United States, January 2006.